Available online at www.sciencedirect.com
SCIENCE DIRECT®
Journal of Power Sources 135 (2004) 9–16
JOURNAL OF POWER SOURCES
www.elsevier.com/locate/jpowsour

Evaluation of the residual stress for anode-supported SOFCs

H. Yakabe [a,*], Y. Baba [a], T. Sakurai [a], Y. Yoshitaka [b]

[a] *Fundamental Technology Research Laboratory, Technical Research Institute, Tokyo Gas Co. Ltd., 16-25 Shibaura, 1-chome, Minato-ku, Tokyo 105-0023, Japan*

[b] *Japan Synchrotron Radiation Research Institute, 1-1-1 Kouto Mikazuki-cho, Sayo-gun, Hyogo 679-5198, Japan*

Received 1 September 2003; received in revised form 19 November 2003; accepted 21 November 2003

Available online 23 July 2004

Abstract

Residual thermal stresses in the electrolyte of the anode-supported planar solid oxide fuel cells (SOFCs) were estimated experimentally and numerically. The X-ray diffraction method was employed to measure the residual stress in the cell. To estimate the residual stress precisely, a synchrotron radiation was used as the best means of X-ray source. The wavelength of the radiation beam used for the stress measurements was 0.154 nm, and the diffraction peak of YSZ (5 3 1) plane was used for the stress measurement. The estimated residual stresses in the electrolyte were compressive stresses of around 650 MPa at room temperature. Numerical calculation for the residual stress was also carried out.

Keywords: SOFC; Residual stress; Anode-supported cell; X-ray stress measurements

1. Introduction

Anode-supported solid oxide fuel cells (SOFCs) are suitable for operations at lower temperatures because of the substantially lower ohmic resistance of the electrolyte. By lowering the operating temperature of SOFCs below 800 °C, conventional metal alloys can be used for interconnectors or auxiliary components with which a high mechanical reliability of a cell-stack and lower manufacturing costs can be achieved. Thus, recently, anode-supported SOFCs are receiving much interest [1–5]. The anode-supported cells are generally fabricated by co-firing the thin electrolyte on the anode substrate at 1400–1500 °C [1–5]. Ni/YSZ and YSZ are used as the anode substrate and the electrolyte, respectively. The thermal expansion coefficients (TEC) of Ni/YSZ and YSZ do not match well, and as a result the mismatch induces a large residual stress in the cell at room temperature. The thermal stress may induce micro-cracks or a delamination of the electrolyte at the interface under a thermal cycle. These damages of the cell decrease the cell performance, and sometimes, cause a destruction of the cell. Thus it is significant to reduce the thermal stress under the thermal cycles.

We have been studying the cell performance and the thermal stresses in the cell using computer simulation for the self-supporting type planar SOFCs [6–8]. Recently we have also carried out numerical analysis on cell performances [9] and thermal stresses on the anode-supported cell. However, for the simulation of the thermal stress, precise calculations are difficult to perform because the residual stresses in the cell at room temperature are not known well. Hence estimating the residual stresses in the electrolyte of the anode-supported cells at room temperature is useful for the calculation of the thermal stresses in the anode-supported cell under cell operations.

In this paper, we report the evaluation of the residual stresses in the electrolyte of the anode-supported cell at room temperature. The X-ray diffraction method was used to measure the residual stresses in the electrolyte of the anode-supported cell, and a synchrotron radiation was used as an excellent X-ray source, which enables the estimation of the residual stresses in the electrolyte with a high accuracy. We also carried out a numerical calculation for the residual stresses in the electrolyte of the anode-supported cell, and made clear that the calculated stresses were close to those experimentally measured.

2. Experimental

We measured the X-ray diffraction pattern for the electrolyte of the anode-supported cell, and estimated the residual stresses by the $\sin^2\psi$ method [10–14]. When a sample is sustaining stresses, the interplanar spacing d between the

* Corresponding author. Tel.: +81-3-5484-4828; fax: +81-3-3453-7583.
E-mail address: yakabe@tokyo-gas.co.jp (H. Yakabe).

0378-7753/$ – see front matter © 2004 Elsevier B.V. All rights reserved.
doi:10.1016/j.jpowsour.2003.11.049

specified diffracting planes of a crystallite in a microscopic grain can be expressed as

$$d = \frac{1+\nu}{E} d_0 \sigma \sin^2\psi + \left\{1 - \frac{\nu}{E}(\sigma_1 + \sigma_2)\right\} d_0 \quad (1)$$

where d_0 is the interplanar spacing under a stress-free condition, ψ the tilting angle of the specified diffracting plane in the crystallite from the normal to the sample surface, ν the Poisson's ratio, E the Young's modulus, σ the stress in the grain, and σ_1 and σ_2 are the principal stresses [10–13]. Modifying Eq. (1), σ is expressed by

$$\sigma = \frac{E}{(1+\nu)} \frac{1}{d_0} \frac{\partial d}{\partial \sin^2\psi} \quad (2)$$

To derive Eq. (2), it is assumed that the sample is isotropic and elastic. In addition, there is no stress perpendicular to the sample surface, because only the stresses near the sample surface are measured using the X-ray diffraction method.

In this stress measurement we employed the iso-inclination method and the fixed ψ_0 method. The configuration for the diffraction measurements and the stress analyses is indicated in Fig. 1. In Fig. 1, ψ_0 is the angle between the normal to the sample surface and the incident beam and 2θ is the scattering angle of the specified diffracting plane in the crystallite. In the fixed ψ_0 method, 2θ scan is carried out at a fixed ψ_0. We determine $+\psi$ and $-\psi$ as follows ($+\psi$; the sample normal is tilting to the diffraction beam, $-\psi$; the sample normal is tilting to the incident beam). To eliminate the effect of an orientation of the crystalline or an irregularity of the grain on the stress measurements, the sample was fluctuated by $\pm 1^\circ$ around the fixed ψ_0 with an enough high speed compared with the scanning speed of 2θ.

A synchrotron radiation was used as an X-ray source. The synchrotron radiation is an ultra-bright, highly directional, and collimated light. In addition, a wide spectrum of wavelengths, stretching from infrared to X-rays can be used. Using the synchrotron radiation as the beam source in the residual stress measurements has the following advantages [14]:

1. The beam with an arbitrary wavelength is available and thus the stress measurement for an arbitrary diffracting plane with a high accuracy is possible.
2. The beam is the monochromatic light and thus it is not necessary to consider the effect of $K_{\alpha 1,\alpha 2}$ doublet.

The experiment was performed at BL09XU line at SPring-8, which is a standard X-ray undulator beam line. For the stress measurements, we selected an X-ray energy of 8.05 keV ($\lambda = 0.1541$ nm), which corresponds to the Cu Kα line, to compare the present results with those measured using a commercial X-ray diffraction apparatus. The attenuation length of the X-ray of $\lambda = 0.1541$ nm in ZrO_2 at a fixed angle of 90° is calculated to be around 15 μm. The typical thickness of the electrolyte was around 30 μm, which is almost triple the attenuation length of the X-ray in ZrO_2, and thus, the contribution of the anode to the diffraction beam was negligible.

The beam size at the sample point was adjusted to 1 mm (H) × 1 mm (V) using W slits. Regarding the diffracting plane used for the stress measurements, we selected (5 3 1) plane of 8YSZ.

The anode-supported cells used for the stress measurements were fabricated by co-firing both the electrolyte and the anode at 1500 °C [15]. The 8YSZ electrolyte was first screen printed, or dip-coated on the green NiO/YSZ substrate. To avoid generations of cracks and micro-pores in the electrolyte, the particle sizes of the raw powders for NiO/YSZ substrate and YSZ electrolyte were selected carefully. After co-firing, the anode-supported cell was cooled down to room temperature. The typical cell size was 40 mm × 40 mm × 2 mm, and the thickness of the electrolyte was about 20–40 μm (the image is shown in Fig. 2). As compared to the anode substrate, the electrolyte is thin enough to assume that the direction of the main stress in the electrolyte is parallel to the film surface. To investigate the stress distribution in the anode-supported cell, two 10 mm × 10 mm pieces were cut from the center and the corner parts of the sample. In this measurement, we

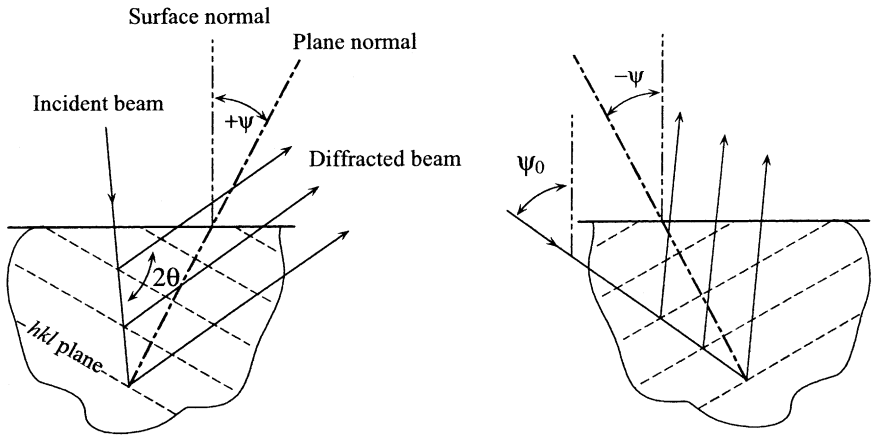

Fig. 1. Schematic diagram of the X-ray stress measurement; iso-inclination method and fixed ψ_0 method.

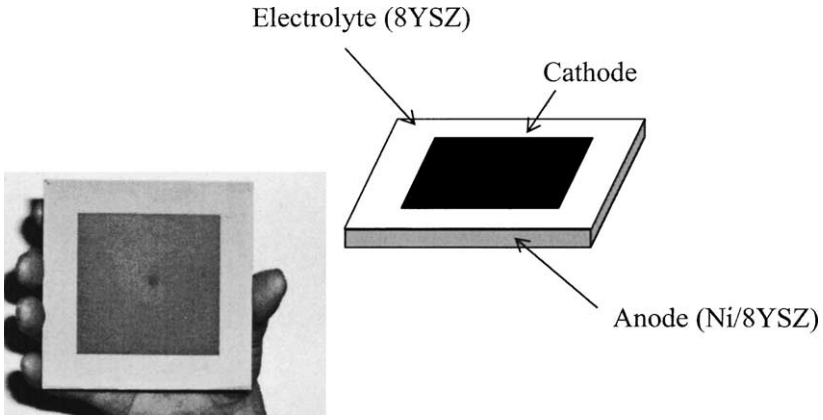

Fig. 2. Schematic view of the anode-supported cell.

Table 1
List of the properties of the samples used for the stress measurement

ID	Electrolyte material	Manufacturing process	Post treatment	Anode state	Position
1	8YSZ	Screen-print	As-sintered	Oxidized	Center
2	8YSZ	Screen-print	As-sintered	Oxidized	Corner
3	8YSZ	Screen-print	Flattened	Oxidized	Center
4	8YSZ	Screen-print	Flattened	Oxidized	Corner
5	8YSZ	Screen-print	Flattened	Reduced	Center
6	8YSZ	Screen-print	Flattened	Reduced	Corner
7	8YSZ	Dip-coat	Flattened	Oxidized	Corner

measured the residual stresses for seven different samples. The characteristics of the samples are listed in Table 1. Samples 1 and 2 were cut from an as-grown cell. Usually, the as-grown cell warped toward the electrolyte side as shown in Fig. 3. If the cells warp, it is difficult to contact each cell well, and the electric connection between cells becomes poor. Hence, we reformed the warp and flattened the cell using a distributed load on the electrolyte at 1400 °C.

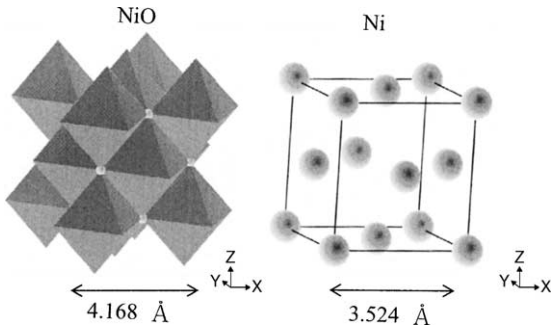

Fig. 4. Comparison of the lattice structure and the relevant lattice constant between NiO and Ni.

Samples 3 and 4 were cut from the flattened cell. Before an operation of the cell, the anode part of the cell has to be exposed to a reducing atmosphere to reduce NiO to Ni in the anode. Samples 5 and 6 were the reduced samples. The lattice constant of Ni is smaller by 20% than that of NiO as illustrated in Fig. 4. As a result, the reduction of the anode

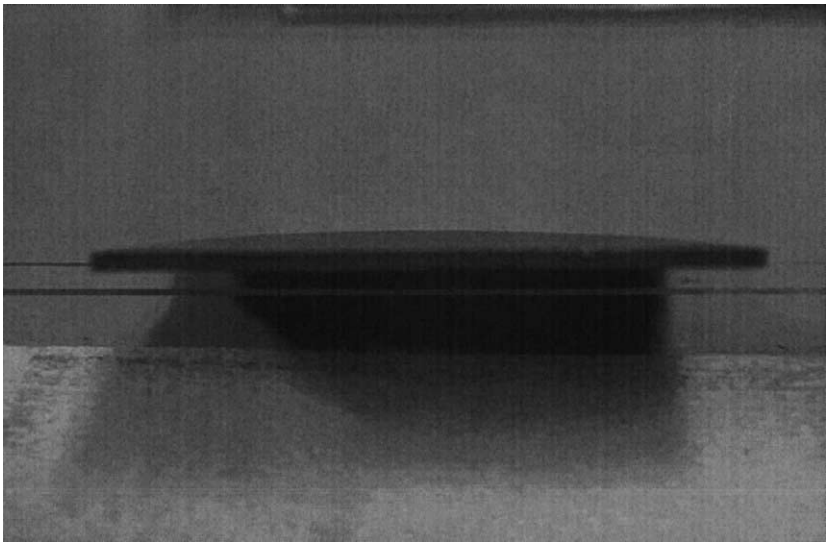

Fig. 3. Side view of the warped anode-supported cell. The electrolyte is located at the upper side.

Table 2
List of the mechanical properties and cell size used for the stress simulation

	Young's modulus (GPa)	Poisson's ratio	TEC (K^{-1})	Thickness (mm)
Electrolyte	206[a]	0.3[b]	10.56×10^{-6}[c]	$40 \times 40 \times 0.03$
Anode	96[d]	0.3[b]	12.22×10^{-6}[c]	$40 \times 40 \times 2$

[a] Taken from Ref. [16].
[b] Assumed value.
[c] Assumed from the temperature dependence of TEC below 1000 °C [8].
[d] From 4-point bending tests at room temperature.

causes a shrinkage of the anode, and may change the residual stress in the electrolyte. For Samples 1–6, the electrolyte is screen printed on the surface of the anode substrate first and then co-fired. Only for Sample 7, the electrolyte was dip-coated on the surface of the anode substrate.

Numerical calculations for the thermal stresses in the anode-supported cells were carried out using the finite element program "ABAQUS" (Hibbit, Karlsson and Sorensen Inc.). We modeled the geometry of the cell of the electrolyte/anode bi-layer, and calculated the residual thermal stresses at room temperature. In the calculation, we assumed that both the electrolyte and the anode were constrained each other below 1400 °C, and the origin of the residual stresses in the cell was only the mismatch of TEC between the electrolyte and the anode. The mechanical properties and the cell size used for the stress calculation are listed in Table 2.

3. Results and discussion

Fig. 5 shows the result of θ–2θ scan for the electrolyte of the Sample 3. First the sample was set so that the sample surface was parallel to the incident beam, and then the incident beam was spotted at the center part of the sample. All the peaks in the diffraction pattern can be assigned to the cubic YSZ structure. There are no diffraction peaks from the anode substrate.

Fig. 6 displays the change of the diffraction peak of YSZ (5 3 1) plane with the change of ψ measured for the Sample 3. With increasing ψ, the peak position shifts to the higher angle, indicating that the inter-planar spacing d decreases and the stress type is compressive. To determine the center of the peak, the peak profiles are fitted with the Gaussian-function, and, thus produced d–$\sin^2\psi$ diagram is shown in Fig. 7. The open circles and open squares are for the positive and the negative ψ, respectively, and the solid line is the linear least-squares fit. Although the data are slightly scattered, d decreases linearly with the increase of $\sin^2\psi$. From the slope of the d–$\sin^2\psi$ diagram, the residual stress can be estimated using Eq. (2). In the X-ray stress measurements, the stress in a sample can be estimated using the diffraction from the specified diffracting plane of crystallites which orients to the specified direction. Therefore the elastic constant E and ν in Eq. (2) is different from those measured by a mechanical method, and, this elastic constant should be measured using the X-ray diffraction method. In this study, however, it was difficult to measure E and ν for the practical cell by the X-ray diffraction method. Since there are no data for the X-ray elastic constant measured using YSZ (5 3 1) plane, we calculated the elastic constant assuming the Voight model [12,17] using the reported elastic constant for cubic YSZ [18]. The reported elastic constant for cubic YSZ and the calculated $E/(1+\nu)$ are listed in Table 3. For the Sample 3, the estimated residual stress in the electrolyte was a compressive stress of 633 MPa. For all the other samples, the estimated residual stresses in the electrolyte are listed in Table 4. From the present results, the following information was obtained.

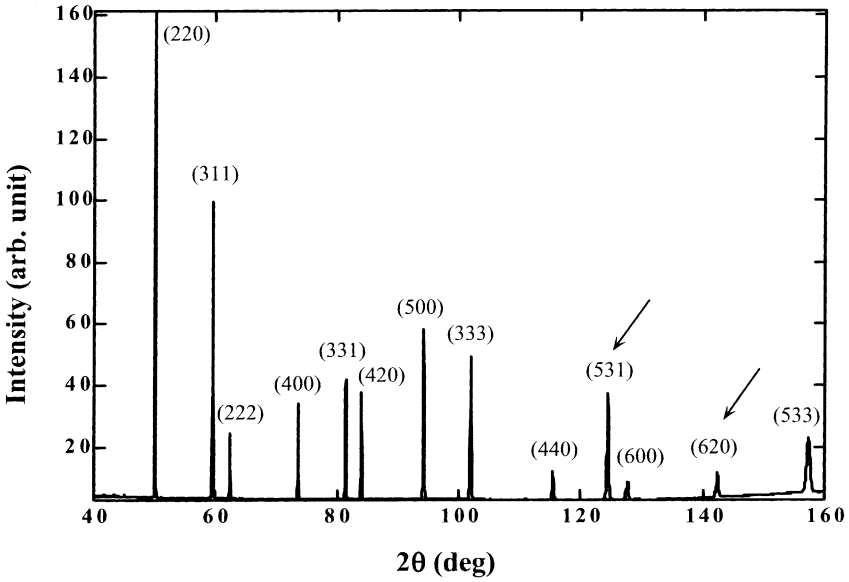

Fig. 5. X-ray diffraction pattern for the electrolyte of the anode-supported cell.

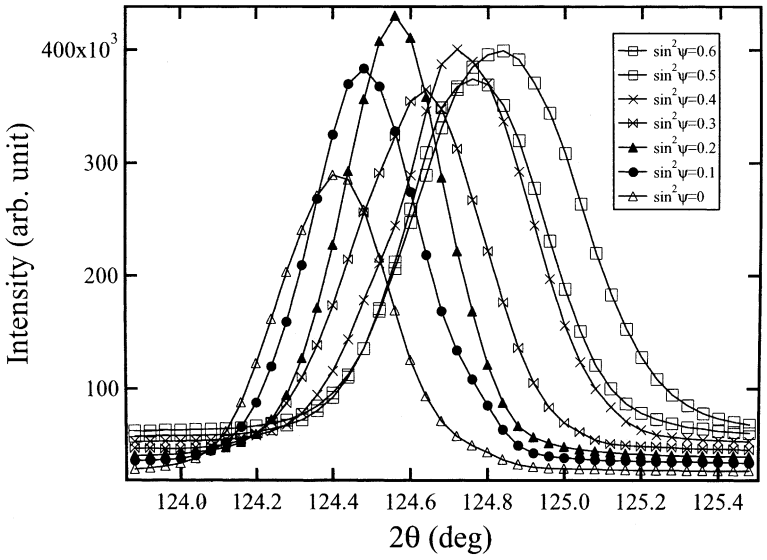

Fig. 6. Change of the diffraction peak of YSZ (5 3 0) plane with the change of ψ for the Sample 3.

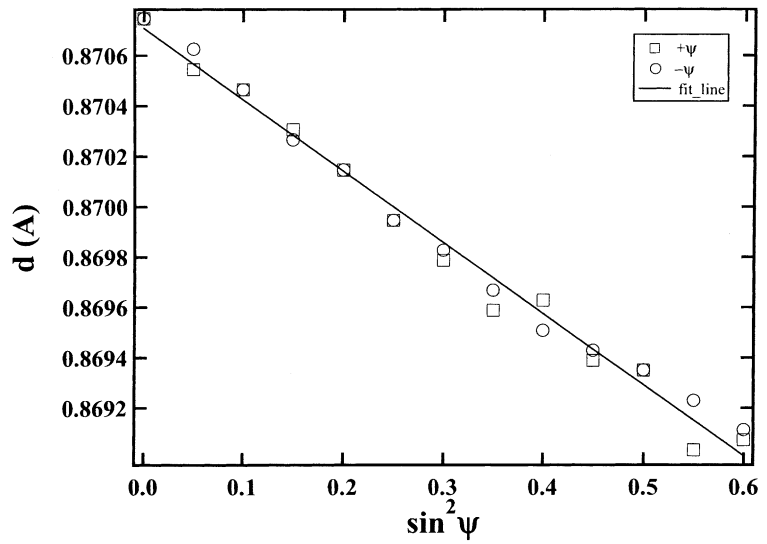

Fig. 7. d–$\sin^2\psi$ diagram measured for the Sample 3; open circles and open squares are for the positive and the negative ψ, respectively, solid line is the linear least-squares fit. d was determined from the diffraction peak of YSZ (5 3 0) plane.

(a) By comparing 1 and 2, the residual stress was larger at the center part of the cell. The origin of the difference was the macro deformation of the cell (i.e. the warp of the cell).
(b) By the flattening treatment, the residual stress at the center part of the cell was lowered, and the distribution of the residual stress in the electrolyte became small. This means that the electrolyte is in a plastic state at 1400 °C.
(c) The effect of the reducing treatment of the anode on the residual stress is small. This may come from that the Young's modulus of the anode became small owing to the reduction. That is, the effects of the softening of the anode may just cancel the effect of the expansion on the residual stress.

Table 3
List of the stiffness of the cubic YSZ used for the calculation of the elastic constant

	C_{11} (GPa)	C_{12} (GPa)	C_{44} (GPa)	$E/(1+\nu)$ ($\times 10^{-4}$ GPa^{-1})
Electrolyte	400[a]	110[a]	55[a]	182

[a] Taken from Ref. [18].

Table 4
List of the results of the simulation for the residual stress in the electrolyte

Sample ID	1	2	3	4	5	6	7
Calculated stress (MPa)	774	672	633	677	658	678	676

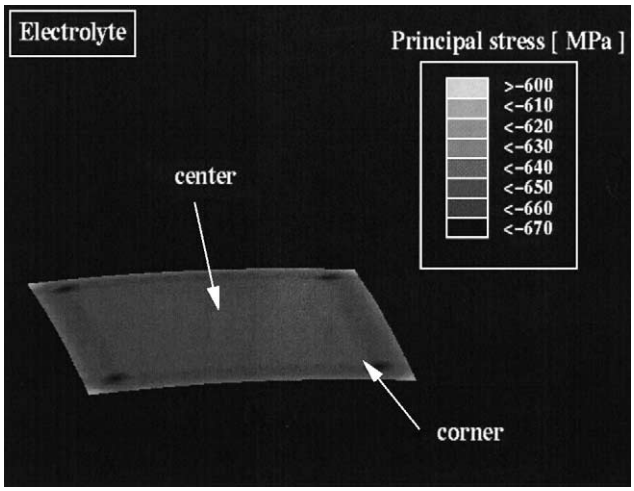

Fig. 8. Simulated stress distribution in the electrolyte at room temperature.

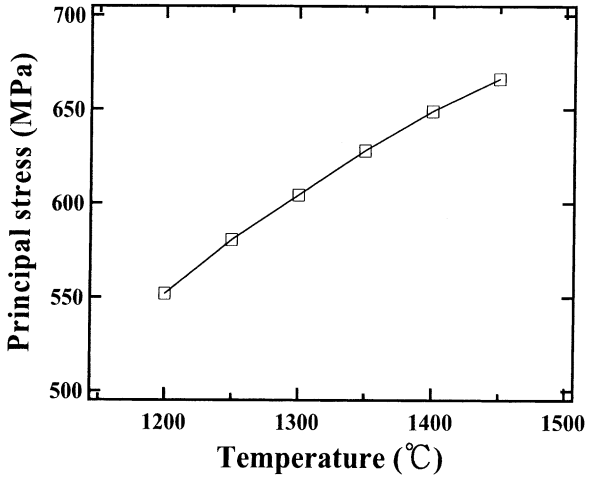

Fig. 9. Effect of the temperature at which the electrolyte and the anode are constrained on the calculated residual stress in the electrolyte.

(d) The residual stress is independent of the fabrication method of the electrolyte. This is reasonable because the origin of the residual stress may be only the mismatch of TEC between the electrolyte and the anode.

Numerical simulations for the residual stresses in the cell at room temperature were also carried out to check the validity of the stress measurement. The sample geometry used for the simulation was the same as the practical cell used for the X-ray stress measurements. Fig. 8 shows the simulated stress distribution in the electrolyte for the anode-supported cell. This simulation corresponds to the flattened sample. Except for the edge part, the stresses are almost homogeneous values of 640–700 MPa over the electrolyte plane. Near the corner part the stress is slightly larger than that at the center part, which is qualitatively consistent with the result of the X-ray stress measurements. In this calculation, the electrolyte and the anode is assumed to be constrained to each other at 1400 °C. However, the temperature at which the electrolyte and the anode are constrained is not clear, and the assumption of the temperature affects the results of the simulation as shown in Fig. 9. With the change of the temperature at which the electrolyte and the anode are constrained, the calculated stress at the center part varies from 550 to 670 MPa. From the following fact, the temperature at which the electrolyte and the anode are constrained seems to be between 1250 and 1400 °C. The cell could be flattened at 1400 °C, and, the present stress measurement revealed that the flattening treatment did not affect the residual stress, suggesting that the electrolyte and the anode may be constrained below 1400 °C. In contrast, it was reported that the sintering of YSZ does not proceed well below 1250 °C [19]. When the temperature at which the electrolyte and the anode are constrained is assumed to be 1400 °C, the calculated residual stress is close to the measured value. Thus, in the following stress calculations we assumed that the electrolyte and the anode would be constrained at 1400 °C.

Here we will focus on the effect of the cut of the sample on the residual stress. In the stress measurements, the cell was cut into the 10 mm × 10 mm sample. This came from the restriction of the size of the sample stage. It should be taken into account that the cut of the cell would change the residual stress in the sample. Hence using the stress simulation we studied the effect of the sample cut on the residual stress. In the present simulation, the thicknesses of the electrolyte and the anode were fixed to 30 μm and 2 mm, respectively, and the residual stress was calculated with various plane sizes. The result of the simulation is displayed in Fig. 10. When the cell size is more than 5 mm, the calculated stress is almost independent of the cell size. In the practical stress measurements, the sizes of the samples were larger than 5 mm, and, if macro deformations of the sample

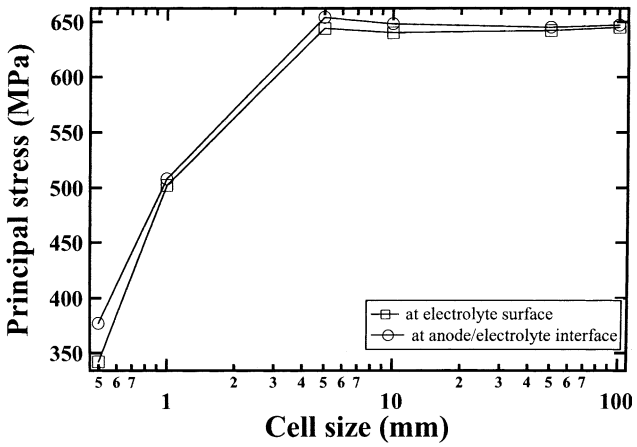

Fig. 10. Effect of the plane sample size on the calculated residual stress in the electrolyte. The thicknesses of the electrolyte and the anode are fixed to 30 μm and 2 mm, respectively.

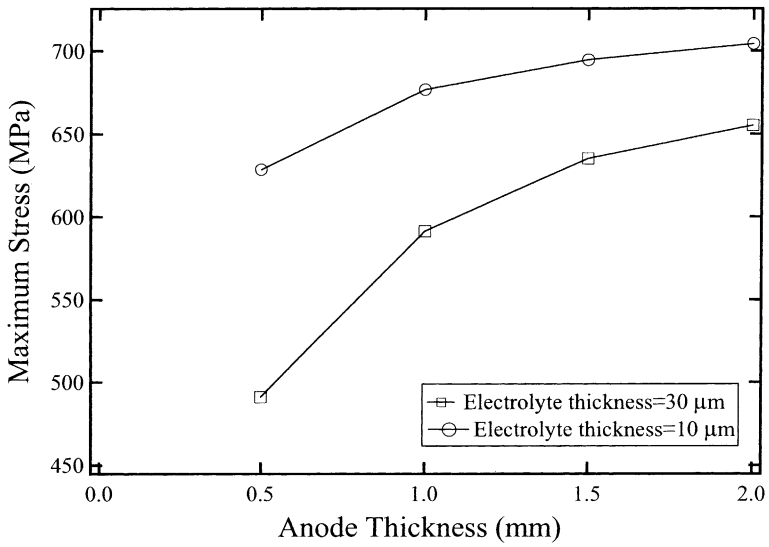

Fig. 11. Effect of the thicknesses of the electrolyte and the anode on the calculated stress in the electrolyte. The plane sample size is fixed to 40 mm × 40 mm.

(e.g. the warp of the cell) hardly affect the residual stress, the effect of the sample cut on the residual stress may be negligible.

Next, we will comment on the effect of the thickness of the electrolyte and the anode on the residual stresses. The residual stresses in the electrolyte were calculated for the difference combination of the thicknesses of the anode and the electrolyte, and the results were displayed in Fig. 11. The combination of the thin anode and the thick electrolyte simply decreases the residual stress in the electrolyte. On the other hand, for a practical cell, the thick electrolyte causes an increase of the electric resistance in the electrolyte. Thus the optimal thickness of the electrolyte has to be selected with consideration of both the electric resistance and the residual stress.

From the X-ray stress measurements and the stress simulation for the electrolyte of the anode-supported cell, it has been made clear that the residual stresses in the electrolyte at room temperature are compressive stresses of around 650 MPa. The strength of YSZ against the compressive stress is more than 1 GPa [20] and thus these residual stresses are not so large as to induce a failure of the electrolyte.

4. Conclusion

The residual stresses in the electrolyte of the anode-supported planar SOFCs were estimated by experimental and numerical methods. The stress measurements were performed by the X-ray stress measurement, and the numerical calculations of the stress were carried out by the finite element method. The estimated residual stresses in the electrolyte were compressive stresses of around 650 MPa. The effects of the cell geometry, the flattening treatment, the fabrication method of the electrolyte, and the reduction of the anode on the residual stress were also studied.

Acknowledgements

The synchrotron radiation experiments were performed at the SPring-8 with the approval of the Japan Synchrotron Radiation Research Institute (JASRI) (Proposal No. 2001A0239-ND-np).

References

[1] S. Primdahl, M.J. Jorgensen, C. Bagger, B. Kindl, in: Proceedings of Solid Oxide Fuel Cells VI, 1999, p. 793.
[2] J.P. Ouweltjes, F.P.F. van Berkel, P. Nammensma, G.M. Chrisite, in: Proceedings of Solid Oxide Fuel Cells VI, 1999, p. 803.
[3] D. Stover, U. Diekmann, U. Flesch, H. Kabs, W.J. Quadakkers, F. Tietz, I.C. Vinke, in: Proceedings of Solid Oxide Fuel Cells VI, 1999, p. 812.
[4] Grobal Thermoelectric Inc., Abstracts of 2002 Fuel Cell Seminar, 2002, p. 974.
[5] J.W. Stevenson, P. Singh, Abstracts of 2002 Fuel Cell Seminar, 2002, p. 890.
[6] H. Yakabe, T. Ogiwara, I. Yasuda, M. Hishinuma, in: Proceedings of Solid Oxide Fuel Cells VI, 1999, p. 1087.
[7] H. Yakabe, T. Ogiwara, I. Yasuda, M. Hishinuma, in: Proceedings of the Third International Fuel Cell Conference, 1999, p. 357.
[8] T. Ogiwara, H. Yakabe, M. Hishinuma, I. Yasuda, in: Proceedings of European Solid Oxide Fuel Cell Forum IV, 2000, p. 193.
[9] H. Yakabe, M. Hishinuma, M. Uratani, Y. Matsuzaki, I. Yasuda, J. Power Sources 86 (2000) 423.
[10] I.C. Noyan, J.B. Cohen, Mater. Sci. Eng. 75 (1983) 179.
[11] I.C. Noyan, J.B. Cohen, Adv. X-Ray Anal. 27 (1984) 129.
[12] K. Tanaka, Y. Yamamori, N. Mine, K. Suzuki, in: Proceedings of the 32nd Japan Congress on Materials Research, 1989, p. 199.
[13] Y. Yoshioka, Adv. X-Ray Anal. 24 (1981) 167.

[14] M. Barral, J.M. Sprauel, J. Lebrun, G. Maeder, S. Megtert, Adv. X-Ray Anal. 27 (1984) 149.
[15] I. Yasuda, M. Uratani, K. Itoh, H. Yakabe, Y. Matsuzaki, Abstracts of Fuel Cell Seminar, 2000, p. 574.
[16] H. Greiner, E. Keim, W. Kleinlein, E. Wei, in: Proceedings of the Solid Oxide Fuel Cell II, 1991, p. 705.
[17] W. Voight, Lehrbuch der Kristallphysik, Tebubner, Berlin, 1928, p. 962.
[18] B.J. Botha, J.C.H. Chiang, P.M. Mjawara, P.E. Ngoepe, J. Appl. Phys. 73 (11) (1993) 7268.
[19] S.P.S. Badwal, M.J. Bannister, R.H.J. Hannink (Eds.), Science and Technology of Zirconia V, Technology Publishing Company Inc., 1993.
[20] T. Kato, N.S. Wang, A. Negishi, A. Momma, Y. Kasuga, K. Nozaki, in: Proceedings of the Third International Fuel Cell Conference, 1999, p. 461.